MOMENTUM CALCULATIONS IN CRATER FORMATION AND THE MODELING OF IMPACT PROCESSES

B. A. Arkhipov and Yu. S. Stepanov

Zhurnal Prikladnoi Mekhaniki i Tekhnicheskoi Fiziki, No. 3, pp. 120–126, 1965

ABSTRACT: The authors present the results of experiments to determine the dependence of the coefficient ξ, which takes into account the nonstationarity of the impact process, on the impact velocity and the properties of the target and projectile material. Data are obtained on the depth of penetration of low-melting modeling materials into semi-infinite targets; these data are then used to verify previously proposed modeling parameters.

1. In [2] one of the authors, using the expression for the momentum of the material ejected when a crater is formed in semi-infinite target derived by K. P. Stanyukovich [1], proposed a scheme for the penetration of an individual target.

The total momentum J_n transferred to the target is equal to the sum of the backward momentum J_R of the mass M ejected during cratering and the momentum of the projectile (particle) J_0. At high impact velocities v_0 we have $J_n \gg J_0$ [1], and therefore in [2] it was considered that

$$J_n \approx J_R, \qquad J_n = J_R + J_0, \qquad J_R = \xi \sqrt{2ME_0},$$
$$\xi = J_R [(m_0 + m_1)(m_0 v_0^2 - 2Q)]^{-1/2}. \tag{1.1}$$

Here ξ is a coefficient taking into account the nonstationarity of the process, E_0 is the kinetic energy of the projectile, m_0 is the mass of the projectile, m_1 the mass of the ejected target material, Q is the initial energy of the projectile lost to the latent heats of phase transitions.

At large v_0, when the projectile is completely vaporized, and assuming that the crater is hemispherical [2],

$$Q = m_0 q_0^{**} + \frac{2\pi r_*^3 \rho_1 p_0}{3 p_1^{**}} \left(q_1^{**} - q_1^* + q_1^* \frac{p_1^{**}}{p_1^*} \right),$$
$$r_* = \eta r_0, \quad h = r_* \left(\frac{p_0}{H_1} \right)^{1/3}. \tag{1.2}$$

Here q^{**} and q^* are the latent heats of vaporization and fusion, p^{**} and p^* are the pressures at the wave front at which vaporization and fusion of the material take place (determined from the Hugoniot relation), ρ is the density of the material, r_* is the effective of the projectile, η is a coefficient characterizing the rearward and lateral unloading, h is the depth of the crater, r_0 is the initial projectile radius, p_0 is the pressure for plane impact ($r_0 \to \infty$), H_1 is the dynamic hardness, and the subscripts 0 and 1 refer to the projectile and the target, respectively.

It should be noted that in (1.2) the latent energy of crushing q_* is neglected, although the volume of destroyed, but not vaporized material removed from the crater is about 80% of its total volume [2]. However, this step is justified, since according to certain data [1] q_* is one to two orders lower than q^{**}.

We now consider some questions of modeling. In [2] Andriankin and Stepanov described a series of dimensionless parameters $\alpha_1, \ldots, \alpha_{17}$, of which, for metals, the variable ones are mainly α_3, α_4, α_6, and α_2 for impact of materials with $\rho_0 \neq \rho_1$. The parameter α_1 serves for converting the velocities of the modeling and modeled materials

$$\alpha_1 = \frac{\rho_1 v_0^2}{H_1}, \quad \alpha_2 = \frac{\rho_0}{\rho_1}, \quad \alpha_3 = \frac{\rho_1 q_1^{**}}{H_1},$$
$$\alpha_4 = c_1 \left(\frac{\rho_1}{H_1} \right)^{1/2}, \quad \alpha_6 = \frac{q_1^{**}}{q_1^*}. \tag{1.3}$$

In the same paper it is also pointed out that in modeling fusion and vaporization, the impact velocities must lie above the threshold velocities of fusion and vaporization of the modeling materials.

We shall determine the threshold velocity v_n from the residual temperature T_+ of the body after the pressure has fallen to $p = p_a$, where p_a is the pressure of the ambient medium. In this case, the phase transition temperature $T^\circ = T_+ = \Delta E_+ / c_V$ at $p = p_a$, where ΔE_+ is the part of the thermal energy remaining in the body after unloading from p_0 to p_a, computed graphically in [3], c_V is the specific heat of the body at $p = p_a$, and v_n corresponds to p_0. Note that the beginning of phase transition corresponds to the temperature at the shock front $T_f = T^\circ(p_f)$, but T° at $p = p_f$ is not known; therefore $E^{+\circ}$ in the equation $E^+ = E^{+\circ} + q^\circ$ is also unknown.

Threshold velocities of vaporization were previously computed in [4, 5]. In this case the threshold velocities were assumed to be those at which the internal energy at the original shock front exceeded the energy of cohesion of the target material. It should be noted that, in accordance with [3],

$$E(V, T) = E^-(V) + E^+(V, T), \tag{1.4}$$

where E^- and E^+ are, respectively, the "cold" and "hot" components of the internal energy, V is specific volume, and T temperature.

The calculated v_n and the the corresponding p_0 are presented in Table 1 for several metals with known equations of state. Clearly, for the modeling metals (Cd, Pb, Sn, Zn), the threshold velocities v_n are considerably lower than for Fe and Al and lie in the laboratory range of impact velocities. It also follows from Table 1 that the values of the threshold velocities of vaporization are in satisfactory agreement with the values computed in [4].

2. For the experimental measurement of J_R we used a ballistic pendulum. The scheme for determining J_R will be clear from Fig. 1. The notation is as follows: O is the point of suspension of the ballistic pendulum (friction in the hinge is neglected), α is the deflection angle of the pendulum, R its length from the point of suspension to the center of gravity, and S the horizontal deflection of the pendulum.

Table 1

Metal pair	Fusion		Vaporization			
	$p_0 \cdot 10^{-12}$, bar	v_n, km/sec	$p_0 \cdot 10^{-12}$, bar	v_n, km/sec	$p_0 \cdot 10^{-12}$, bar	v_n, km/sec [4]
Fe → Fe	2.0	5.94	3.0	7.73	2.91	7.6
Al → Al	0.7	5.72	1.5	9.37	1.25	8.35
Cd → Cd	0.28	1.72	0.5	2.55	0.57	2.8
Pb → Pb	0.25	1.41	0.6	2.64	0.66	2.8
Sn → Sn	0.2	1.53	1.0	4.58	—	—
Zn → Zn	0.4	2.37	0.7	3.44	0.81	3.8

Then, if α is determined from experiment,

$$J_R = m\,[2gR\,(1-\cos\alpha)]^{1/2}, \quad m = M_0 + P_1. \tag{2.1}$$

Here M_0 is the mass of the pendulum itself, P_1 is the mass of the target at the end of the swing, when the cratering process is complete, and G is the acceleration of gravity. P_1 should not be replaced by the initial mass of the target P_0, since the main fraction of J_R is transferred to the target at the beginning of the cratering process [1, 2]. Since S/R is small (for small α)

$$(1 - S^2/R^2)^{1/2} \approx 1 - S^2/2R^2$$

and from Fig. 1 it follows that

$$AC = \frac{S^2}{2R}, \qquad J_R = mS\left(\frac{g}{R}\right)^{1/2}. \tag{2.2}$$

Measuring α and S experimentally, one can calculate J_R from (2.1) and (2.2).

In the experiments we used targets made of Cd, Bi, Sn, Pb, Sb, Zn, Al, Fe, P-500 polyethylene, sodium butadiene rubber, butyl rubber, polysiobutylene, RK-9 obturator rubber, and poroloh. The results were used to determine ξ and to check the modeling method based on parameters (1.3). As projectiles we used pellets of diameter d_0 = 10 mm made of the above-mentioned materials, except for the polymers. The radii and heights of the metal targets were usually an order greater than the diameter of the projectile, so that they could be assumed to be semi-infinite (in the absence of lateral expansion of the targets). The polymer targets were usually penetrated completely; therefore values of ξ were not obtained for these materials (except for RK-9 rubber).

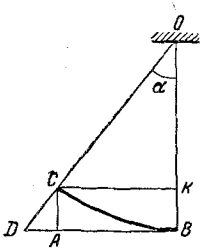

Fig. 1

The volume of the crater to the level of the original surface and to the rim was measured correct to 0.1 ml using a dropping buret. All the geometric measurements (diameter of surface around crater raised above original level, diameter of crater at level of rim and at level of starting surface, height of rim cross section of crater, maximum depth of crater) were made directly after the experiment on a special pattern, which made it possible to refer all the vertical dimensions to the same base. The values of P_0 and P_1 were determined by weighing correct to 0.01 g. This accuracy was necessary, since sometimes the loss of weight of the target m_1 was very slight (for craters of relatively large volume, the compaction of the material at the crater walls was considerable).

To measure the velocities we used wire probes on frame-targets triggered by the breaking of an electrical circuit. The signals were fed to a "Neptune"-type electronic chronometer which gave readings of time intervals correct to 0.25 μsec (BG 1.409.003. TO). Generally, we used two "Neptunes" for two measuring bases with four frame-targets, so as to duplicate the measurements. The pendulum and the frame-targets were placed in a special box to prevent contamination of the room with chemically toxic substances. The weight of the pendulum was about 200 kg, M_0 = 13.475 kg, R = 65.1 cm. The propulsion system employed made it possible to accelerate the projectiles to velocities $v_0 \sim 3.5$–4 km/sec were obtained with the aid of a hydrogen-driven light-gas ballistic apparatus.

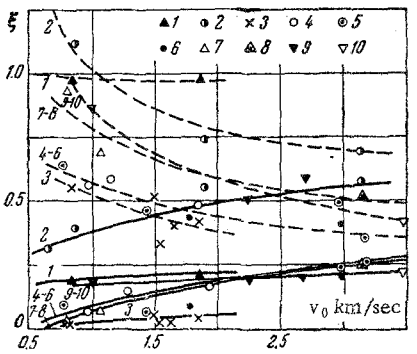

Fig. 2

3. The results of the experiments are presented in Figs. 2–5. Figure 6 shows some of the specimens after cratering. At subthreshold impact velocities, in order to compute ξ, it is necessary to know the value of q_*. In view of the absence of direct data on the latent energies of crushing q_* for the materials employed, the coefficient ξ was calculated from possible variants of the determination of q_*.

The coefficient ξ_1 is the least value of ξ calculated without account for projectile kinetic energy losses (Q = 0). In [1] the value of q_* for certain metals and nonmetals was taken as 10^9 erg/g. The coefficient ξ_2 was computed under this assumption with allowance for the energy losses in both the target and the projectile. In the calculations the original parameters on both sides of the impact boundary were computed by the graphic deceleration method [3]. The coefficient ξ_3 was calculated under the assumption $q_* = H_1/\rho_1$. In this case the values of q_* are of the order of 10^9 erg/g (they are presented in Table 2).

If it is assumed that all the internal energy at the initial shock front is expended on crushing the target (at $v_0 < v_n$), then the values of ξ obtained give the upper limit of the range of true values of ξ. However, these values will evidently be too high.

In order to compute the value of q_*, it is necessary to know the behavior of the compressive stress-strain diagram for the material in the

Table 2

Metal	H_1, kg/mm^2	$q_* \cdot 10^{-9}$, erg/g	Metal	H_1, kg/mm^2	$q_* \cdot 10^{-9}$, erg/g	Metal	H_1, kg/mm^2	$q_* \cdot 10^{-9}$, erg/g
ST 45	250	3.18	ST 40 Kh	480	6.1	Sb	110	1.5
ST 30	180	2.29	D — 16 T	90	3.3	Cd	59	0.682
ST 20	315	4	Sn	42	0.577	Zn	144.5	2.02
Armco	185	2.35	Bi	23	0.235	Pb	11	0.097

Note. The data on H_1 not published in [2, 14–16] were obtained from the penetration of a rigid cone.

elastoplastic loading region and the value of the final density ρ_2 at the the walls of the crater. Then

$$q_* = \int_{\varepsilon_1}^{\varepsilon_2} \sigma(\varepsilon)\, d\varepsilon .$$

Here σ is the stress, ε_1 the strain corresponding to the end of the elastic zone of loading, ε_2 the strain corresponding to ρ_2. For most of the materials used in our work, data on the dynamic compression diagram in the elastoplastic region are not available, the only exceptions being low-carbon steel and aluminum [6, 7].

$$q_* = \frac{1}{2} p_2(\rho_2) \frac{\rho_2 - \rho_1}{\rho_2 \rho_1} . \qquad (3.2)$$

For the calculated averaged values of the final parameters in the target p_2, ρ_2 the losses Q, computed under the assumption (3.2), were so small that the results for ξ were actually close to ξ_1. Since, as it turned out, in the presence of fusion and vaporization the quantity q_* can be neglected as compared with q^* and q^{**}, for $v_0 < v_n$ it was subsequently assumed that $\xi \approx \xi_1$.

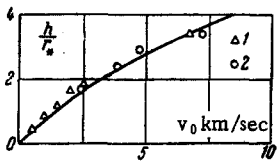

Fig. 3

Figure 2 shows values of ξ for the investigated materials in the range of impact velocities obtained (each isthe averaged result of several experiments). For comparison the relation

$$\xi^\circ = J_n [(m_0 + m_1)(m_0 v_0^2 - 2Q)]^{-1/2}$$

is shown by a broken line (J_n is the total measured momentum), corresponding to points ξ calculated from (1.1).

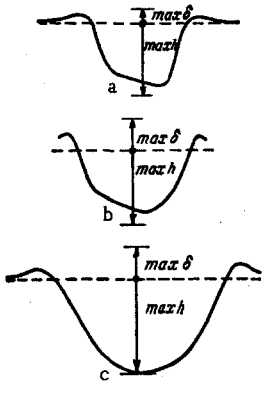

Fig. 4

The relations $\xi(v_0)$ and $\xi^\circ(v_0)$ are monotone and become increasingly smooth with increase in v_0. It may be assumed that their common asymptote lies between them, and in the limit, if equation (1.1) is satisfied, they merge. The metal with the greatest scatter in the values of ξ is zinc, this evidently being attributable to its greater brittleness as compared with the more ductile cadmium, lead, and tin. In Fig. 2 the following notation is used:

1 — ST3 → ST45, *2* — ST3 → D16T, *3* — Zn → Zn, *4* — Cd → Cd

5 — Fe → Cd, *6* — D16T → Cd, *7* — Sn → Sn, *8* — Fe → Sn

9 — Pb → Pb *10* — Fe → Pb

For a semi-infinite target of RK-9 rubber the values of ξ were about 0.8, i.e., higher than for metals at the same velocities. Semi-infinite targets of cadmium, tin, and lead were subjected to the impact of pellets 10 mm in diameter of the same materials and steel, and cadmium was also exposed to the impact of cylinders of duralumin with effective radius $r_* = 6.5$ mm. In this case, as may be seen from Fig. 2, the results for ξ lie satisfactorily close to a single curve, which may be regarded in the first approximation as confirmation of the fact that ξ is a physical characteristic of the target material and does not depend on the density, dimensions, and shape of the projectile. It should be noted that the curve $\xi(v_0)$ for steel and duralumin is well extrapolated to the curve $\xi(v_0)$ for cadmium and tin at impact velocities calculated with the corresponding conversion factor, which indicates the possibility of modeling with respect to ξ also (cadmium and tin model mark ST-3 steel and mark D-16T duralumin [2]). Before the experiments we tested the parametric modeling method on the modeling materials themselves [2]. By way of illustration we present the data on h for several experiments using the parameter α_4 (in the range $v_0 < v_n$):

Cd → Cd, $v_0 = 0.987$ km/sec, $h = 1.15$ cm, $m_0 = 4.84$ g,

$d_0 = 1.02$ cm Zn → Zn (131° C), $v_0 = 1.523$ km/sec,

$h = 1.15$ cm, $m_0 = 3.72$ g, $d_0 = 1.0$ cm.

For heated zinc with allowance for the dependence $H_1(T)$ [2]

ST-3 → ST-3, $v_0 = 1.785$ km/sec, $h = 0.93$ cm, $m_0 = 4.13$ g,

$d_0 = 1.0$ cm Zn → Zn, $v_0 = 1.75$ km/sec, $h = 1.08$ cm,

$m_0 = 3.77$ g, $d_0 = 0.99$ cm $v_{0Fe} = 1.065\, v_{0Zn}$.

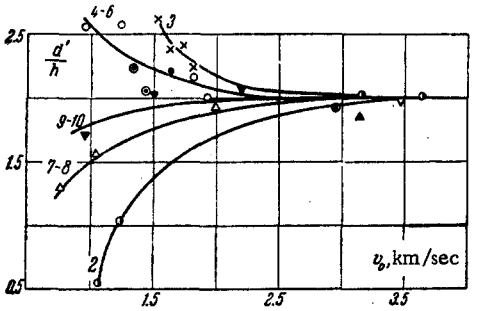

Fig. 5

An attempt was made to test the modeling method on pairs of different metals. However, it failed, since it proved extremely difficult to select equal ratios α_2. Thus, for example, with respect to the parameter α_4 the pair Bi → Sn models the pair Fe → Al

($H_{Fe} = 315$ kg/mm^2 $H_{Al} = 250$ kg/mm^2

$\alpha_{4Fe}/\alpha_{4Al} = 1.18$, $\alpha_{4Bi}/\alpha_{4Sn} = 1.09$, $v_{0Fe} = 2.73 v_{0Bi}$).

The velocity conversion factor was determined from the relation

$$\left(\frac{\rho_0 v_0^2}{H_1}\right)_{Fe \to Al} = \left(\frac{\rho_0 v_0^2}{H_1}\right)_{Bi \to Sn} .$$

In this case the h for these pairs differs by more than four times. This indicates the importance of the parameter α_2 at subthreshold impact velocities. In Fig. 3 experimental values for Cd → Cd with velocity conversion ($v_{0Fe} = 2.43 v_{0Cd}$) have been plotted on the graph of $h/r_*(v_0)$ for Fe → Fe [2] (1—experimental data of [8, 9]); it is clear that the modeling is satisfactory.

In [2] and in certain other work it was assumed that $p_2 = H_1$ (p_2 and ρ_2 are the final values of the pressure and density at the wave front in the target at the end of crater formation), and the depths of the craters at high impact velocities were calculated on this assumption (from

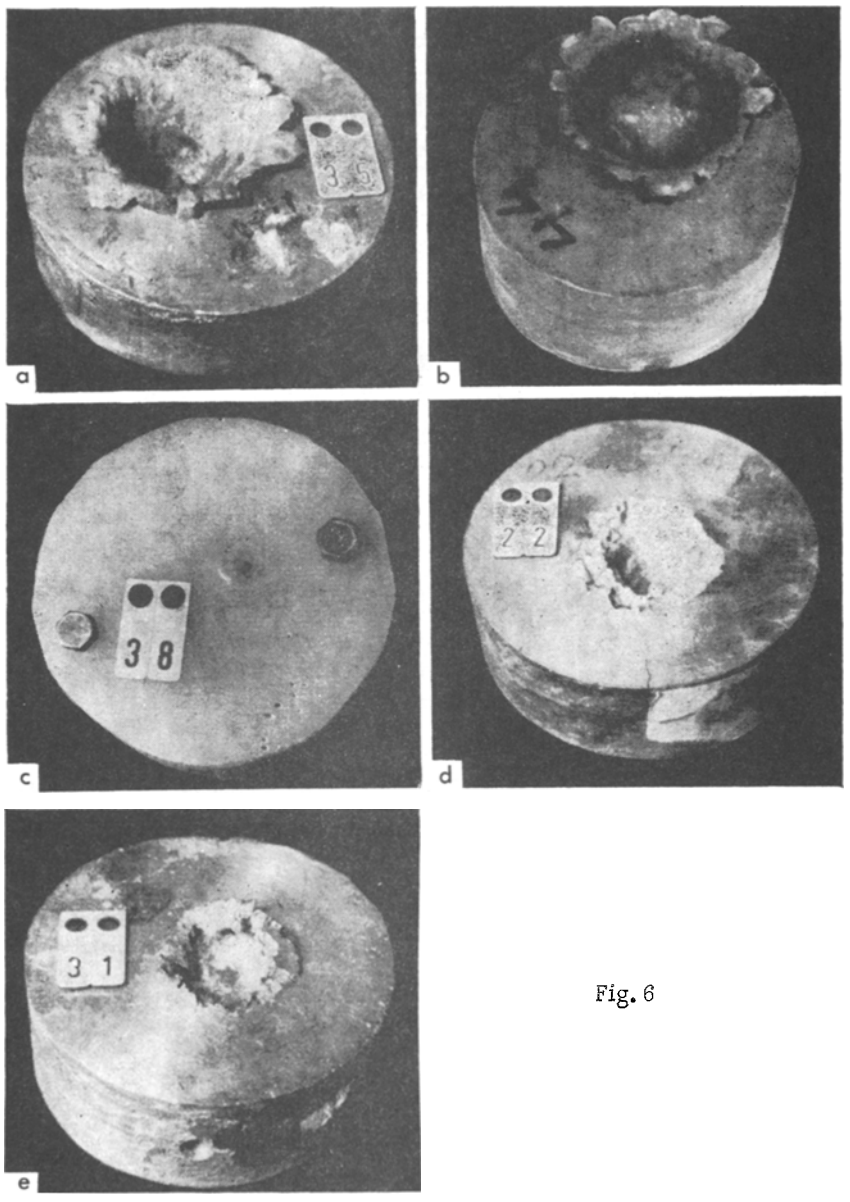

Fig. 6

(1.2)). These calculations are in satisfactory agreement with the existing experimental data [8, 9]. In order to verify the correctness of the above criterion $p_2 = H_1$, it is necessary to determine ρ_2 experimentally and to know the compression diagram for the material in the region of elastoplastic strains. If V_2 is the volume of the crater determined experimentally, and V_0 the initial volume of the target, then the end density ρ_2° is not generally equal to ρ_2, since instead of V_0 it is necessary to put $V_0' < V_0$, and instead of P_1, $P_1' < P_1$ (P_1, and V_0' are the weight and volume of the part of the target near the walls of the crater in which $\varepsilon_2 \geq \varepsilon \geq \varepsilon_1$). We note also that the experimentally determined density of the material in the walls of the crater after its formation and unloading to the pressure of the ambient medium must be somewhat less than the density ρ_2 of the material compressed behind the shock wave.

The final pressure p_2 for ST-3 with $\varepsilon = 1 - \rho_1/\rho_2^\circ$ was determined from the data of [6], that for D-16T from the data of [7]. For the other metals with know Hugoniot adiabatics we took

$$p_2 = \rho_1 D_1 u_1, \qquad u_1 = \frac{c_1(\sigma - 1)}{\lambda_1 - (\lambda_1 - 1)\sigma},$$

$$\sigma = \frac{\rho_2^\circ}{\rho_1}, \qquad D_1 = c_1 + \lambda_1 u_1. \tag{3.4}$$

Here D and u are the wave and mass velocities, c and λ are constants characterizing the shock adiabatic. For these q_* from (3.2) was calculated for p_2 obtained from (3.4). The values of p_2 obtained were somewhat lower than H_1 for ST-3 and D-16T, which indicates the great significance of the zone of elastoplastic strains in crater formation

However, these data should be regarded as preliminary owing to the absence of values P_1' and V_0'. At small impact velocities, when the projectile is only slightly deformed, the following logarithmic relation is valid for the penetration depth [10, 11]:

$$h = \frac{2m_0}{\pi\rho_1 d_0^2 k_0} \ln\left(1 + k_0\rho_1 \frac{v_0^2}{H_1}\right) (k_0 - \text{Shape factor}). \tag{3.5}$$

As shown by a comparison of the experimental data and calculations based on (3.5), the latter is valid up to the following velocities v_0: Pb → Pb, $v_0 \sim 1$ km/sec; Sn → Sn, $v_0 \sim 1.2$ km/sec; Zn → Zn, $v_0 \sim 1.8$ km/sec. These velocities correspond roughly to crushing of the projectile.

It is of some interest to study the variation of crater shape with velocity. Thus, Fig. 4 shows cross sections of craters for the pair Sn → Sn at different velocities. Figure 4, a – $m_0 = 3.95$ g, $v_0 = 0.794$ km/sec; Fig. 4, b – $m_0 = 3.62$ g, $v_0 = 1.045$ km/sec (target preheated to T = 146° C); Fig. 4, c – $m_0 = 3.74$ g, $v_0 = 2.0$ km/sec, the broken line denotes the level of the starting surface, max δ the maximum height of the crater rim, max h the maximum crater depth. The crater cross sections were taken in an arbitrary plane. Figure 5 shows the ratio of the diameter d' of the crater at the level of the starting surface to its depth below the starting surface h plotted against the impact velocity. In this case the notations correspond to those of Fig. 2. Clearly, with increase in v_0 the shape of the crater approaches the hemispherical. This is also confirmed by other experiments [12].† The possible asymmetry of the crater cross section was caused by a slight inclination in the direction of impact with respect to the surface of the target. From Figs. 4a and 4b it is clear that in a heated target the height of the crater rim is much increased for roughly the same impact velocity v_0. At the same time, heating has almost no effect on the depth of the crater. It should be noted that an almost "cup-like" [13] crater shape is obtained for $\rho_0 > \rho_1$ at low velocities, when the projectile is not crushed and the crater is formed by penetration of the projectile, and not by the destructive action of the shock front (directed action).

An example of this is offered by the pair Fe → Al. Plastic flow of the material has a considerable effect on the shape of the crater. Figures 6, a, b show craters in lead:

Pb → Pb, $m_0 = 6.04$ g, $d_0 = 1.0$ cm, $h = 2.4$ cm, $d' = 4.0$ cm, $v_0 = 0.987$ km/sec Fe → Pb, $m_0 = 3.5$ g, $d_0 = 0.95$ cm, $h = 3.65$ cm, $d' = 6.3$ cm, $v_0 = 3.5$ km/sec.

Clearly, there is still a gap between the bent-down lobes of the rim and the starting surface, which indicates a high degree of plastic flow in the lead (in the presence of fusion bent-down lobes would not be formed). Polymer targets were found to have an interesting property. The holes resulting from penetration of the target were partially or completely filled in. In the case of butyl rubber and polyisobutylene the holes were resealed completely, even at relatively high velocities $v_0 \sim$ ~ 3.5–4 km/sec upon penetration by a steel pellet $d_0 \sim 1.2$ cm. Figure 6c shows the complete penetration of a polyethylene specimen by a steel pellet with $d_0 = 1.0$ cm at $v_0 = 0.972$ km/sec. The initial hole has been reduced to a diameter of ~ 2 mm which evidently indicates intense local heating of the walls of the opening. Figures 6d, and 6e show craters in zinc targets obtained under roughly the same conditions (v_0 = = 1.64 and 1.523 km/sec, respectively); in experiment No. 31 the target was first heated to 131° C. Clearly, in the heated target spallation of the surface is much reduced. Since moderate heating leads to almost no change in the rate of propagation of the front face depends on interference of the opposing compression and rarefaction waves to a lesser extent than spallation of the rear face. Evidently, heating reduces the relaxation time, which leads to a more rapid transition of the hot, as compared with the cold, material into the plastic state, so that spallation of the front face is prevented. On the right of the crater in experiment No. 31, the spalled material was unable to break away and thus remained in a "blistered" state. The results of the above experiments may be summarized as follows.

1. The relation $\xi(v_0)$ is a characteristic of the target material and is practically independent of the density, shape, and size of the projectile; ξ decreases with increase in the density of the target material for constant impact velocity v_0.

2. The relation $\xi(v_0)$ is monotone increasing and at $J_n \gg J$ tends to a limiting value.

3. The modeling parameters obtained in [2], including those for firing at heated targets, are shown to be correct.

4. With increase in v_0, the shape of the crater tends toward the hemispherical.

It should be noted that the above conclusions are valid in the limited range of impact velocities obtained experimentally.

The authors thank E. I. Andriankin for discussing the results.

REFERENCES

1. K. P. Stanyukovich, "Elements of the theory of impact of solid bodies at high (cosmic) velocities," Iskusstv. sputn. Zemli, no. 4, p. 86, 1960.

2. E. I. Andriankin and Yu. S. Stepanov, "Penetration depth on meteoroid impact," Iskusstv. sputn. Zemli, no. 15, p. 44, 1963.

3. L. V. Al'tshuler, K. K. Krupnikov, B. N. Ledenev, V. I. Zhuchikhin, and M. I. Brazhnik, "Dynamic compressibility and equation of state of iron at high pressures," ZhETF, vol. 34, no. 4, p. 874, 1958.

4. N. A. Zlatin, "On the theory of high-velocity impact on metal," ZhTF, vol. 31, no. 8, p. 982, 1961.

5. M. A. Cook, "Mechanism of cratering in ultra-high velocity impact," J. Appl. Phys., vol. 30, no. 5, p. 725, 1959.

6. Yu. S. Stepanov, "Determination of the compressive stress-strain diagram for low-carbon steel in the region of elastoplastic strains," PMTF, no. 3, p. 116, 1963.

7. K. B. Broberg, Shock Waves in Elastic and Elastoplastic Media [in Russian], Gostekhizdat, 1959.

8. W. S. Partridge H. B. Vanfleet and C. R. Whited, "Crater formation in metallic targets," Appl. Phys., vol. 29, no. 9, p. 1032, 1958.

†Note added in proof: Additional experimental verifications at high v_0 showed that curve 2 in Fig. 5 lies below that indicated: $d'/h \sim$ ~ 1 at $v_0 \sim 4$ km/sec.

9. R. L. Bjork, "Effect of a meteroid impact on steel and aluminum in space," Proc. X-th Internat. Astronaut. Congress, Springer Verlag, Vienna, vol. 2, p. 505, 1960.

10. I. V. Poncelet "Cours de mechanique industrielle et Rapport sur un memoire de MM Piobert et Morin," Mem. Acad. de Sci., vol. 15, 55, 1829.

11. F. F. Vitman and N. A. Zlatin, "Theory of impact of deformable bodies and the modeling problem," ZhTF, vol. 33, no. 8, p. 982, 1963.

12. R. J. Eichelberger and J. W. Gering, "Effect of meteoriod impacts on space vehicles," ARS J., vol. 32, no. 10, p. 1583, 1962.

13. Yu. P. Raizer, "Motion of a gas under the influence of a concentrated impact at its surface (surface explosion)," PMTF, no. 1, p. 57, 1963.

14. F. F. Vitman, N. A. Zlatin, and B. S. Ioffe, "Deformation resistance of metals at velocities of $10^{-6}-10^{2}$ m/sec," ZhTF, vol. 19, no. 3, p. 300, 1949.

15. F. F. Vitman and V. A. Stepanov, "Effect of rate of deformation on the deformation resistance of metals at impact velocities of $10^{2}-10^{3}$ m/sec," collection: Some Problems of the Strength of Solids [in Russian], izd-vo AN SSSR, 1959.

16. N. N. Davidenkov, F. F. Vitman, and N. A. Zlatin, "Effect of aging of the velocity and temperature dependence of hardness," Symposium in Honor of the 70th Birthday of A. F. Ioffe [in Russian], Izd-vo AN SSSR, p. 307, 1950.

18 August 1964 Moscow